Anal. Chem. **2007,** *79,* 4419−4426

Approach to Detection in Laser-Induced Breakdown Spectroscopy

M. Mueller,*,† I. B. Gornushkin,‡ S. Florek,§ D. Mory,|| and U. Panne†

Federal Institute for Materials Research and Testing (BAM), Richard Willstätter Strasse 11, D-12489 Berlin, Germany, Department of Chemistry, University of Florida, Gainesville, Florida 32611, ISAS Institute for Analytical Sciences, Albert-Einstein-Strasse 9, 12489 Berlin, Germany, and LTB Lasertechnik Berlin, Rudower Chaussee 29, 12489 Berlin, Germany

Gated detection with intensified detectors, e.g., ICCDs, is today the accepted approach for detection of plasma emission in laser-induced breakdown spectroscopy (LIBS). However, these systems are more cost-intensive and less robust than nonintensified CCDs. The objective of this paper is to compare, both theoretically and experimentally, the performance of an intensified (ICCD) and nonintensified (CCD) detectors for detection of plasma emission in LIBS. The CCD is used in combination with a mechanical chopper, which blocks the early continuum radiation from the plasma. The detectors are attached sequentially to an echelle spectrometer under the same experimental conditions. The laser plasma is induced on a series of steel samples under atmospheric conditions. Our results indicate that there is no substantial difference in the performance of the CCD and ICCD. Signal-to-noise ratios and limits of detection achieved with the CCD for Si, Ni, Cr, Mo, Cu, and V in steel are comparable or even better than those obtained with the ICCD. This result is further confirmed by simulation of the plasma emission signal and the corresponding response of the detectors in the limit of quantum (photon) noise.

In the past decade, laser-induced breakdown spectroscopy (LIBS) has challenged an increased interest as an analytical approach to elemental analysis, especially in process analytical applications, microanalysis, and remote sensing (see refs 1 and 2 and references therein).

Since the early days of LIBS, the importance of employing gated intensified detectors, for example, intensified charge-transfer devices (ICCD), to discriminate against the early uncharacteristic plasma emission was emphasized by many authors. Recent works of Carranza et al.,[3] Sabsabi et al.,[4] and Semerok et al.[5] seem to underline again that gated detection with ICCDs outperforms nongated detection with CCDs usually by a factor of 10−100. These comparisons, however, were based on different spectrometer/detector combinations, e.g., a Czerney-Turner spectrometer equipped with an ICCD versus a miniaturized monolithic spectrometer with a CCD.[3,4] A similar detection capability was demonstrated for a nongated CCD and a gated ICCD detector by Bulatov et al.[6] However, different light collection geometries were employed. For the CCD, a side view light collection was used to perform temporally resolved measurements and cut off the initial plasma continuum, whereas top view collection geometry was utilized for the ICCD. In this respect, the employed instrumental setups were not equivalent in spectrometer light throughput and detector performance. Hence, up to now, the published comparisons were more the comparisons of spectroscopic systems rather than of detectors.

From the pertinent literature, one can conclude that, except for a few special cases, CCDs principally provide a better signal-to-noise ratio (SNR) in comparison with ICCDs.[7,8] This is due to a higher quantum efficiency of the CCDs and their lower overall noise. The ICCDs can, however, be advantageous upon detection of very weak signals in the presence of strong background due to their gating capability. As ICCDs are more cost-intensive and less robust than CCDs, LIBS systems based on CCDs would be preferable in many applications.

The objective of this work was to compare a gated intensified CCD with a nongated CCD, which employs a mechanical chopper to cut off the early plasma emission. The performance of both detectors was studied under identical experimental conditions with an echelle spectrometer, which provides a high spectral resolution over an extended spectral range. Due to a simultaneous detection of major, minor, and trace elements in a single echelle spectrum, the dynamic range and spatial resolution of the two-dimensional detectors are of utmost importance in this case. To validate our experimental results, we performed corresponding simulations

* Corresponding author. E-mail: maike.mueller@bam.de.
† Federal Institute for Materials Research and Testing.
‡ University of Florida.
§ ISAS Institute for Analytical Sciences.
|| LTB Lasertechnik Berlin.

(1) Miziolek, A. W., Palleschi, V., Schechter, I., Eds. *Laser-induced Breakdown Spectroscopy (LIBS): Fundamentals and Applications*; Cambridge University Press: Cambridge, 2007.
(2) Cremers, D. A.; Radziemski, L. J. *Handbook of Laser-induced Breakdown Spectroscopy*; John Wiley & Sons: New York, 2006.
(3) Carranza, J. E.; Gibb, E.; Smith, B. W.; Hahn, D. W.; Winefordner, J. D. *Appl. Opt.* **2003**, *42*, 6016−6021.
(4) Sabsabi, M.; Heon, R.; St-Onge, L. *Spectrochim. Acta, Part B: At. Spectrosc.* **2005**, *60*, 1211−1216.
(5) Semerok, A.; Chaleard, C.; Detalle, V.; Lacour, J. L.; Mauchien, P.; Meynadier, P.; Nouvellon, C.; Salle, B.; Palianov, P.; Perdrix, M.; Petite, G. *Appl. Surf. Sci.* **1999**, *139*, 311−314.
(6) Bulatov, V.; Krasniker, R.; Schechter, I. *Anal. Chem.* **2000**, *72*, 2987−2994.
(7) Sweedler, J. V. *CRC Crit. Rev. Anal. Chem.* **1993**, *24*, 59−98.
(8) Sweedler, J. V., Ratzlaff, K. L., Denton, M. B., Eds. *Charge-Transfer Devices in Spectroscopy*; VCH Publishers: New York, 1994.

10.1021/ac0621470 CCC: $37.00
Published on Web 05/16/2007

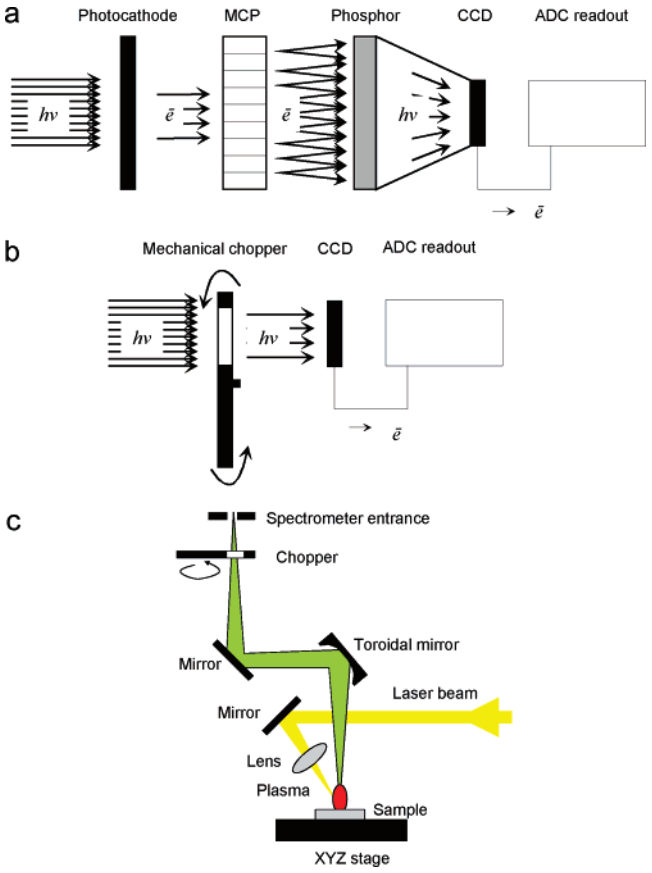

Figure 1. Simplified scheme of the (a) intensified CCD, (b) nonintensified CCD with a mechanical chopper. and (c) excitation/collection geometry.

with a radiative plasma model described earlier.[9−11] The simulations were focused primarily on the expected signal-to-noise performance when employing the two different detector types.

EXPERIMENTAL SECTION

Signal and Noise Considerations for ICCD and CCD Detectors. General working principles of the CCD and ICCD, their design, signal processing, and sources of noise are addressed in refs 7 and 8, Simplified schematics of the ICCD and CCD detectors are depicted in Figure 1a and b; the light collection geometry is given in Figure 1c. It follows from Figure 1a that the conversion of light falling onto the ICCD into an electric signal can be expressed by

$$S = S_{ph} Q_{PC} t G T_p Q_{CCD} \quad (1)$$

where S is the ICCD response (electrons), S_{ph} (photons/s) is the average photon flux incident on the photocathode, Q_{PC} (photoelectrons/photon) is the photocathode quantum efficiency, t (s) is the signal integration time, G (dimensionless) is the gain of the microchannel plate (MCP), T_p (photons/electron) is the efficiency of electron/photon conversion by the phosphor and the image reduction optics (i.e., fiber-optic coupler), and Q_{CCD} (photoelectrons/photon) is the quantum efficiency of the CCD. The signal S expressed in number of electrons is converted to counts in today's ICCDs typically via 1 count ≈ 10 electrons.[8] Although eq 1 presents a simplified version of the full signal-transfer function, nevertheless, it correctly reflects the signal transformation. More advanced analysis can be found elsewhere.[12] For the CCD detector, eq 1 becomes (see Figure 1b)

$$S = S_{ph} t Q_{CCD} \quad (2)$$

In our analysis, the responses expressed via eqs 1 and 2 are used to derive corresponding signal-to-noise ratios that determine the detectors overall sensitivity. The total noise of an ICCD is given by[8]

$$N = (N_R^2 + N_D^2 + N_{EBI}^2 + N_{ph}^2)^{1/2} \quad (3)$$

in which N_R is the readout noise, N_D is the dark current noise, N_{ph} is the photon and MCP shot noise, and N_{EBI} is the photocathode dark noise (equivalent background illumination). Obviously, for the CCD, the term N_{EBI} is absent in eq 3 while the term N_{ph} does not include the MCP noise.

Based on the high quality of the modern detectors (see Table S-1 Supporting Information), short exposure times used in LIBS (μs−ms), and the fact that laser-induced plasma is an extremely bright light source, sources of noise other than photon noise, i.e., the read-out noise, dark current noise, etc., are negligible for both detectors. Even though the exposure time in our experiment was a few orders of magnitude longer for the CCD than for the ICCD, their temperature-dependent dark shot noise was comparable due to the deeper cooling capability of the CCD (−60 versus −20 °C for the ICCD). More strict criteria for the prevalence of the photon noise can be found in ref 12. Equation 3, thus, becomes $N = N_{ph}$.

For a general case, the photon noise is described by the Bose−Einstein statistics

$$\sigma^2 = \langle m \rangle \left[\frac{\exp(h\nu/kT)}{\exp(h\nu/kT) - 1} \right] \quad (4)$$

in which σ^2 is the variance of noise, $h\nu$ is the photon energy, kT is the plasma thermal energy, and $\langle m \rangle$ is the average number of photons per unit time and unit area. For the UV−vis spectral region and moderate temperatures (i.e. $h\nu \gg kT$), eq 4 is reduced to Poisson statistics $\sigma^2 = \langle m \rangle$.

Model of Radiating Plasma and Simulation of Detector Response. A detailed description of the model can be found elsewhere.[9−11] Briefly, the radiation spectrum is calculated for a laser-induced plasma expanding into vacuum. The model is based on a system of gas dynamic equations (Euler equations) coupled with the equation of radiative transfer. Local thermodynamic equilibrium is assumed, allowing the application of the collision-dominated plasma model and standard statistical distributions.

(9) Kazakov, A. Y.; Gornushkin, I. B.; Omenetto, N.; Smith, B. W.; Winefordner, J. D. *Appl. Opt.* **2006**, *45*, 2810−2820.
(10) Gornushkin, I. B.; Kazakov, A. Ya.; Omenetto, N.; Smith, B. W.; Winefordner, J. D. *Spectrochim. Acta, Part B* **2005**, *60*, 215−230.
(11) Gornushkin, I. B.; Kazakov, A. Y.; Omenetto, N.; Smith, B. W.; Winefordner, J. D. *Spectrochim. Acta Part B: At. Spectrosc.* **2004**, *59*, 401−418.
(12) Frenkel, A.; Sartor, M. A.; Wlodawski, M. S. *Appl. Opt.* **1997**, *36*, 5288−5297.

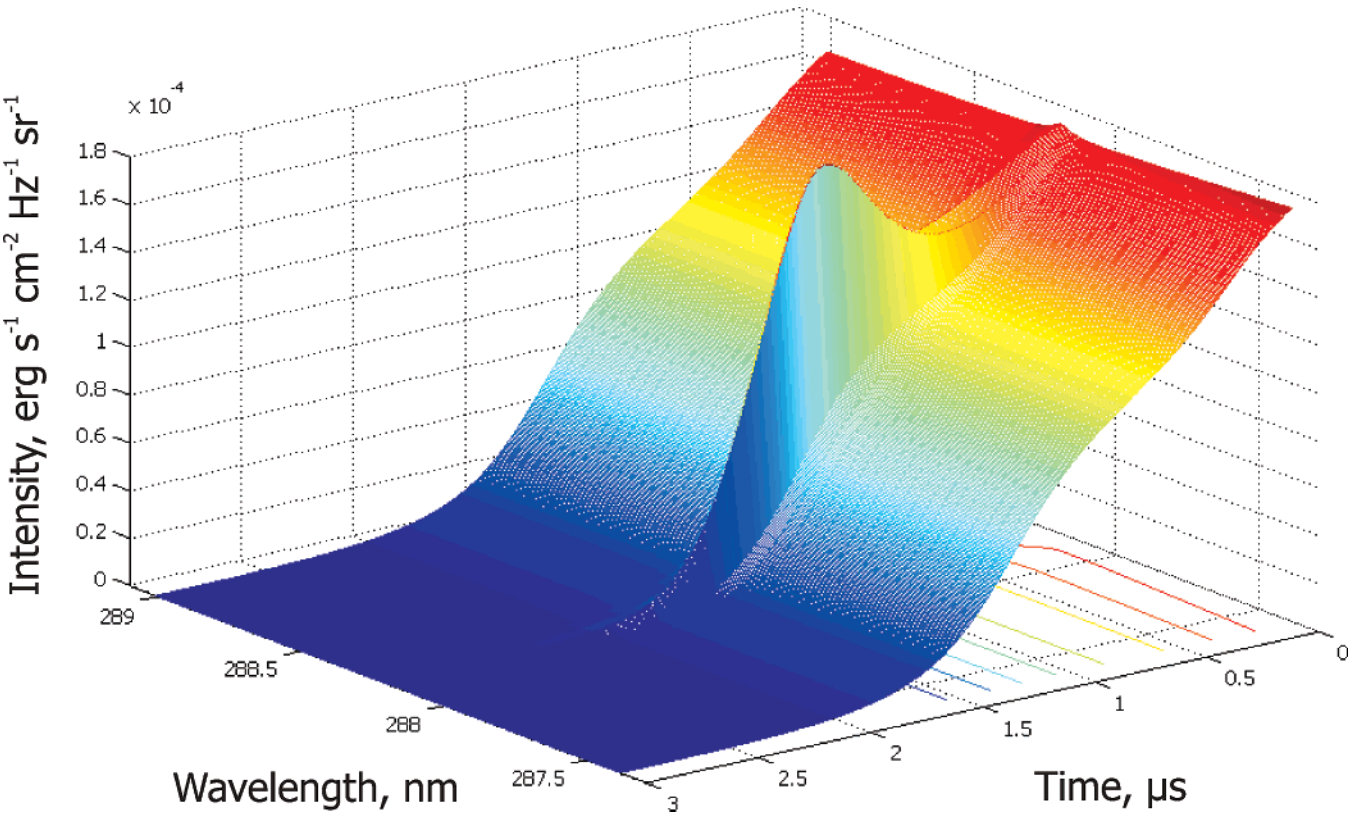

Figure 2. Evolution of plasma spectrum in a narrow spectral interval around Si(I) 288.16-nm emission line. Initial conditions for calculations: $T = 30\,000$ K, $n_{Al} = 4.995 \times 10^{17}$ cm^{-3}, and $n_{Si} = 5 \times 10^{14}$ cm^{-3}.

Based on the dominance of quantum noise for both the CCD and ICCD, the Poisson noise is superimposed on the calculated spectra. The spectral response of a detector is simulated by integrating spectra with the corresponding noise superimposed. For the ICCD, the spectra are integrated within the detector time gate, whereas for the CCD, the integration is performed over the full plasma lifetime starting from the cutoff time of plasma continuum.

The following model input parameters are employed corresponding to the onset of plasma expansion after the laser pulse was terminated and the plasma was thermalized. The initial plasma radius is 15 mm, expansion velocity is 2.5×10^5 cm s^{-1}, initial plasma temperature is 30 000 K, and total initial number density is 5×10^{17} cm^{-3}. The spectra are calculated for the line of sight passing through the plasma center; the initial distributions of plasma temperature and number density are parabolic as in ref 11. A 5 ns time step is used in all calculations, while the total number of time steps is 600, resulting in 3 μs of the total computed plasma expansion.

The calculations are performed for the plasma induced on an aluminum target doped with 0.00025−5% Si, which expands into vacuum. The plasma emission is calculated for the spectral range of 287−290 nm, which includes the strong Si(I) 288.16-nm resonance line. A typical example of the calculated spectral fragment with the Si(I) 288.16-nm line is shown in Figure 2. In the early stage, i.e., 0−0.5 μs, the plasma emission is dominated by strong continuum radiation; the line emission emerges from the emission continuum between 0.5 and 2 μs and slowly decays by ~3 μs. Between the onset of strong line emission and the complete decay of the emission, obviously an optimum time window exists for measuring the characteristic plasma spectrum. The criterion for identification of such a window is the best signal-to-noise ratio as will be described below.

Despite the fact that the simulation is performed for a vacuum plasma induced on a binary material while the experiment is carried out for an atmospheric plasma induced on a multicomponent material, our theoretical results still provide an adequate illustration of the experimental situation. Indeed, the only point of our interest is the response of the two detectors to a transient event. In this respect, the plasma evolves in vacuum similarly to that in an atmosphere, although on a shorter time scale. In both cases, the plasma first exhibits featureless continuum emission and then goes through a stage of strong line emission and then decays in a matter of a few or a few tens of microseconds in vacuum and in atmosphere, correspondingly.

Experimental Setup. A quadrupled Nd:YAG laser (60 mJ maximum pulse energy at 266 nm; Surelite II, Continuum) operating at a 10-Hz pulse repetition rate with a 6-ns pulse width is focused on a sample surface by a convex lens (80-mm focal length) producing a 0.2-mm spot and a corresponding irradiance of ~22 GW cm^{-2}. The incident beam is disposed at an angle of ~8° with respect to the surface normal (see Figure 1c). The sample is placed on a *XYZ* stage inside a sampling chamber positioned in front of the spectrometer. The plasma emission is collected in top view geometry by an inclined toroidal mirror (f = 110 mm) and an additional folding mirror. Both mirrors, coated with a UV-enhanced Al/SiO_2 layer, form a 1:1 plasma image on the entrance slit of an echelle spectrometer (Aryelle; LTB Lasertechnik Berlin GmbH). The Aryelle has a focal length of 400 mm with a numerical aperture of f/10. The system provides

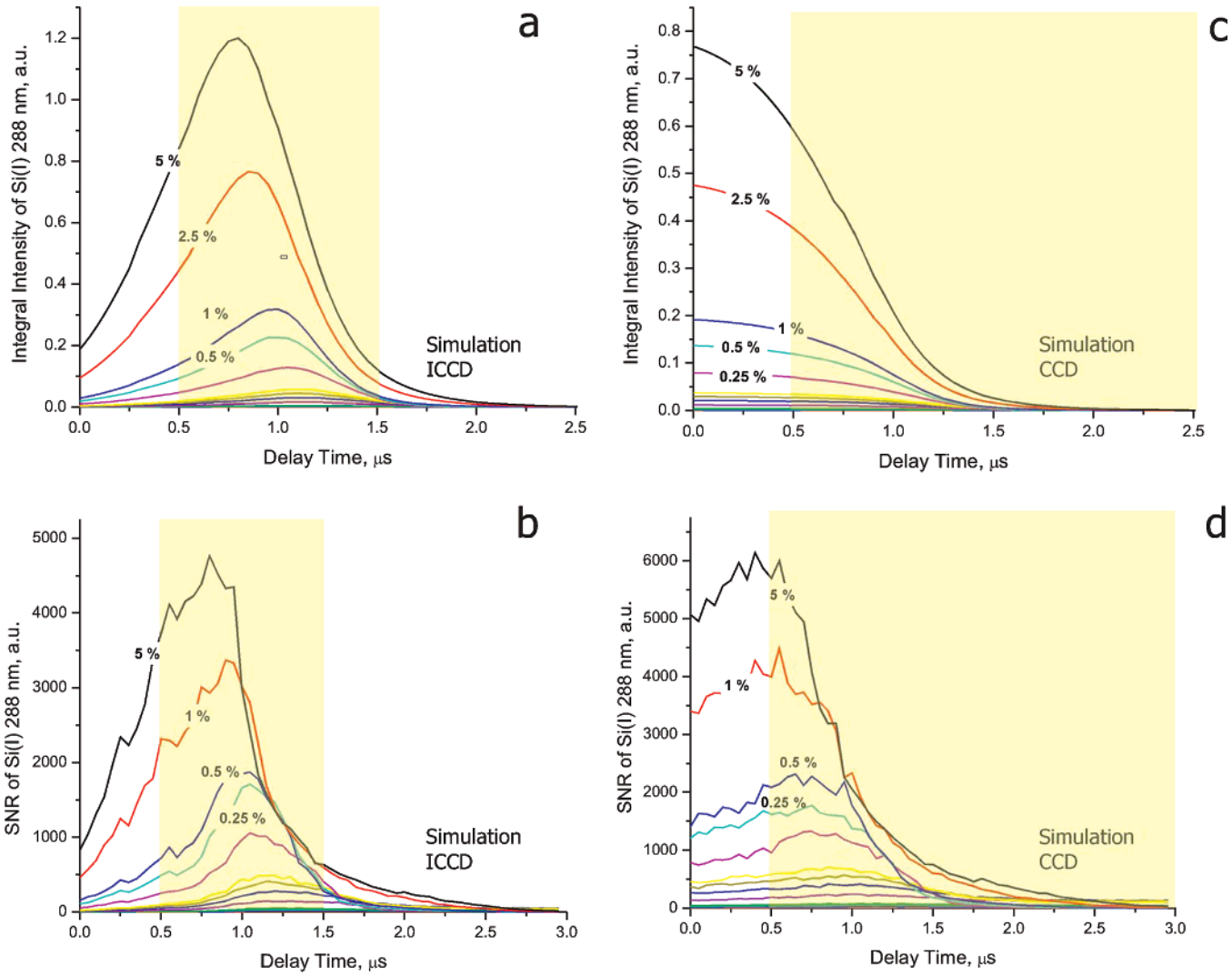

Figure 3. Optimization of theoretical delay time and signal-to-noise ratio for ICCD (a, b) and CCD (c, d) for Si(I) 288.16-nm line in concentration range of 2.5×10^{-4}–5%. Shaded areas define the optimal time window.

an average spectral resolution of $R = 10\,000$ in a broad continuous spectral range between 275 and 780 nm.

Two detectors, the ICCD (DH734-18H-83) and CCD (DV434−BU2), both from Andor Technology, are investigated. Their comparative characteristics are given in Table S-1. The detectors have the same effective area of 13.3×13.3 mm^2; in the ICCD it is provided by a circular 18-mm intensifier and a 1:1 fiber-optical taper. The equal detector areas mean that the results will not be biased by differences in detector geometries. To directly compare the ICCD and CCD for LIBS, the detectors are sequentially attached to the same spectrometer in order to ensure the same light collection geometry. To prevent the CCD from detecting the early plasma continuum, a mechanical chopper is used in front of the entrance slit; for the gated ICCD, the chopper is omitted.

In general, ICCDs yield a slightly lower spatial resolution compared to CCDs because of the optical coupling (by means of a fiber-optical taper) between the MCP and the CCD chip in ICCD detectors. This can result in a reduced spectral resolution of the ICCD-terminated spectrometer working at narrow slits. However, in our case, the selection of a 50-μm entrance slit in the echelle spectrometer results in a slit-limited resolving power of 10 000 providing the identical spectral resolution for both detectors (refer to Figure 1a and b).

Various delays with respect to the incident laser pulse were explored. In case of the ICCD, a photodiode detecting a fraction of the laser light provides a trigger signal, $t = 0$ s, for the photocathode. The nonintensified CCD system was timed through the electronics of a chopper wheel, which provided the trigger ($t = 0$ s) signal for the flash lamp, the Q-switch, and the detector. The chopper provides a minimal rise time of 200 ns and has a 100-ns jitter with respect to the laser pulse.

Samples and Spectra Processing. Nine samples are used of certified low alloy steels (SS 401/1−SS 405/1 SS 406−SS 409, Bureau of Analyzed Samples, Ltd.). The concentrations of the elements analyzed in this paper are given in Table S-2 (Supporting Information).

All spectra are processed using a software written in Matlab 7.2. For theoretical spectra, the background due to continuum radiation is approximated by a second polynomial and subtracted from the gross spectrum, which consists of a line emission superimposed on a plasma continuum (Figure S-1a Supporting Information). For experimental spectra, the background is ap-

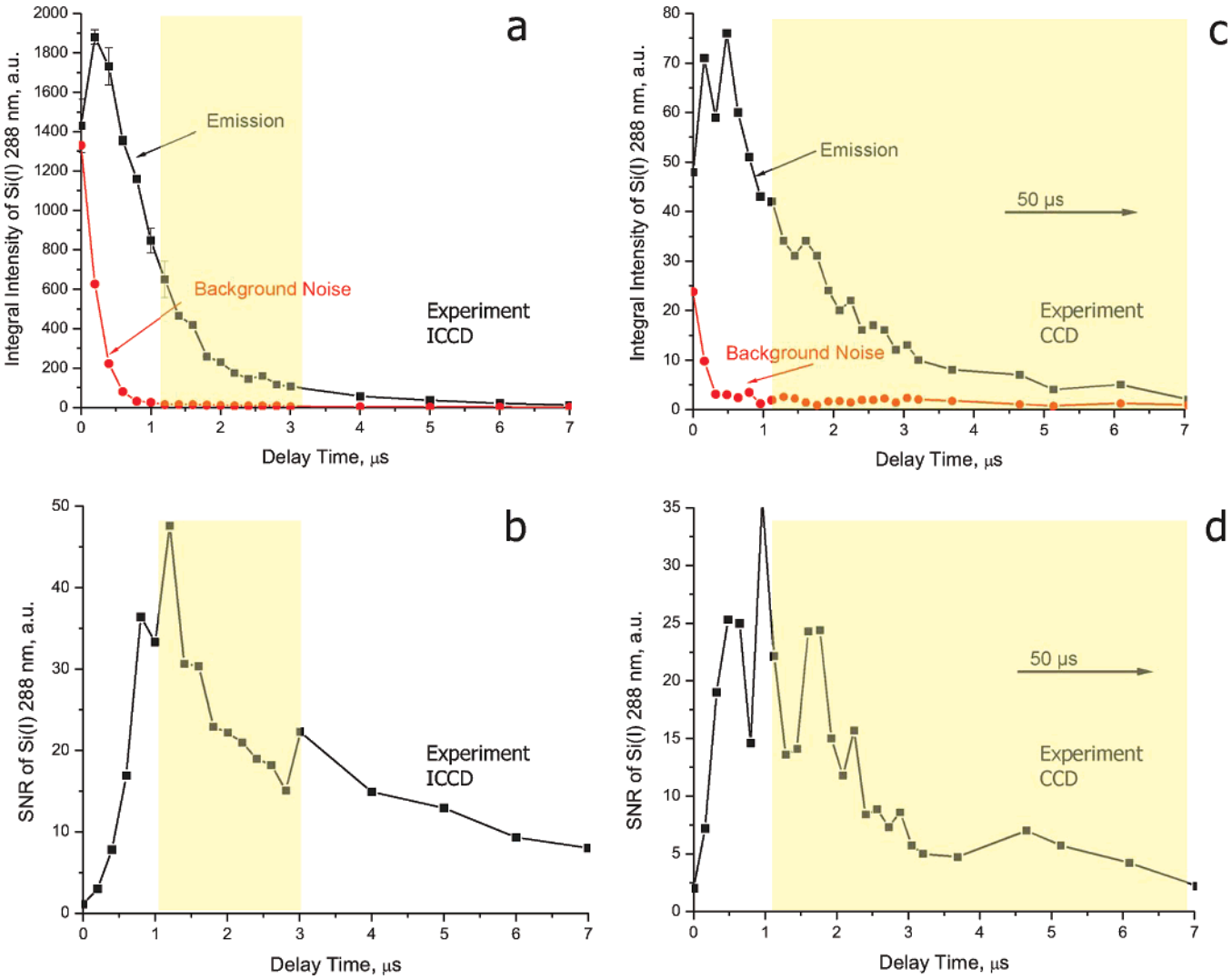

Figure 4. Optimization of experimental delay time and signal-to-noise ratio for the ICCD (a, b) and CCD (c, d) for Si(I) 288.16-nm line. Dots mark the background signal; squares mark the emission signal and SNR. The shaded areas define the optimal time window.

proximated (and then subtracted) by a linear function drawn through the two minimums to the left and to the right of an analytical line (Figure S-1b). The analytical signal is given by a line intensity integrated within the limits of ±1.4 full width at half-maximum as recommended in refs 13 and 14. Emission line profiles are approximated by the Voigt function in theoretical spectra (Figure S-1a) and by the Gaussian function in experimental spectra (Figure S-1b). The latter function adequately described the observed line shapes.

Noise in both cases is determined by fluctuations of the background integrated within the same time and spectral windows as the analytical signal. The spectral region for noise is such that it is free from any specific emission and is located in proximity to the analytical line. Limits of detection (LOD) are calculated based on the convention LOD $= 3\sigma_{Bkg}/m$, in which σ_{Bkg} is describing the standard deviation of the background and m corresponds to the slope of the linear portion of a calibration plot. Experimental calibration plots are forced through zero. The linear regression fit is applied to low concentrations only for which emission lines are not self-absorbed.

RESULTS AND DISCUSSION

Experiment and Model Optimization. The results obtained experimentally using a spectrometer equipped with either a CCD or ICCD are supported by computer simulations. When the CCD is attached to the spectrometer, the mechanical chopper is used to cut off a strong plasma continuum that dominates the plasma spectrum during the first few hundreds of nanoseconds. With the ICCD, the chopper is not necessary because the relocatable gate of the ICCD now determines the acquisition time window. Contrary to the CCD−chopper combination, where only the start time of data collection can be controlled, the gated ICCD allows for control of both the start and end time of data collection.

In laser-induced plasmas, line emission is superimposed on an intense continuum radiation that dominates plasma spectra during the first hundreds of nanoseconds. To cut off the continuum, a gated detector is necessary that gives an obvious advantage to an ICCD over a CCD. However, if the collection start-up time of a CCD is delayed, (e.g., by mechanical chopping), then the SNR for a CCD can become comparable or even higher than that for an ICCD. It is also obvious from analysis of eqs 1−3 that the high gain of an ICCD (G in eq 1) does not yet guarantee a

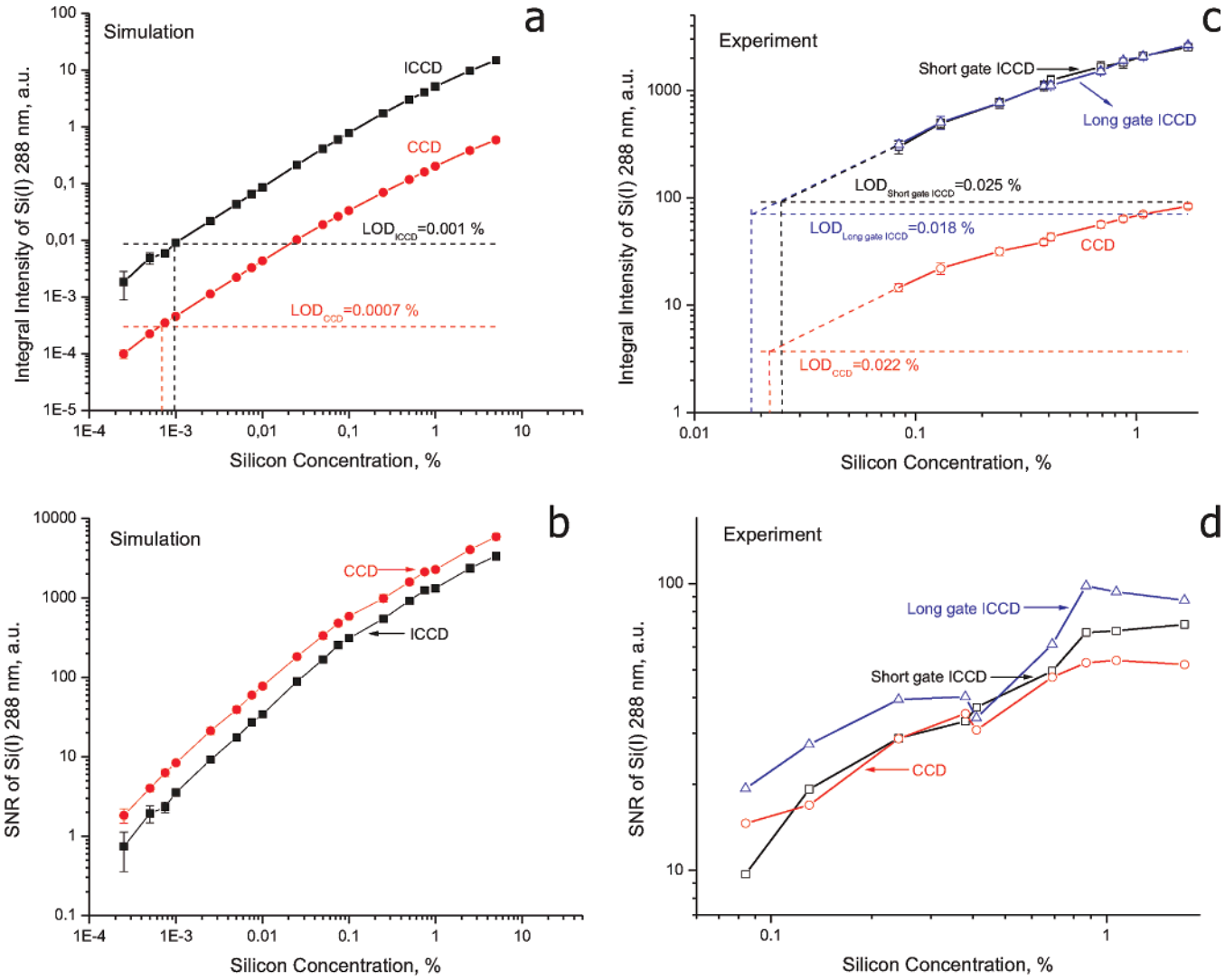

Figure 5. Theoretical calibration plots for Si(I) 288.16 nm in an aluminum matrix (a) and corresponding SNRs (b) for CCD (dots) and ICCD (squares). Experimental calibration plots for Si(I) 288.16 nm in steel (c) and corresponding SNRs (d) for CCD (dots), short gate ICCD (squares), and long gate ICCD (triangles). Dashed lines indicate limit of detection levels.

superior SNR. Photon noise in an ICCD is amplified by the MCP to the same extent as an optical signal. Therefore, the overall higher quantum efficiency of a CCD is able to provide a far better SNR compared to an ICCD.

Another parameter to consider is the dynamic range of a detector. In LIBS applications, a broad dynamic range is highly desirable as it allows simultaneous detection of major and minor plasma components. For both the CCD and ICCD, the dynamic range is limited by the full well capacity of a CCD chip. Obviously, the dynamic range of an ICCD is reduced compared to that of a CCD because the terminal chip in the ICCD detector receives more light due to multiplication of photoelectrons by the MCP.

Optimization of a time-integrated signal is necessary to ensure that the detectors work at a maximum SNR capacity. For the ICCD, an optimum can be found by scanning a narrow time gate over plasma emission lifetime and recording spectra at each position of the gate (i.e., at each delay with respect to the plasma initiation).[13−15] For a nongated detector, such as the CCD with a mechanical chopper, the optimum is found by shifting the initial cutoff time toward later times. The optimal time window is influenced by concentrations of elements (Figure 3) and, more critically, by the temporal behavior of emission lines chosen for analysis.

The results of our *theoretical* delay−gate optimization are shown in Figure 3 where the integral intensities of the Si(I) 288.16-nm line and the corresponding SNRs are plotted as a function of the delay time. For a theoretical ICCD detector, optimization is performed by scanning the 50-ns gate over the 3-μs plasma lifetime in 50-ns increments. A gain of 100 (see Table S-1) of the MCP is assumed throughout all computations. As seen from Figure 3a and b for the theoretical ICCD, the signal and SNR maxima are shifted toward early delay times with the increase of Si concentration. It is clear that upon the integration this shift should be accounted for. Thus, the theoretical integration time window for the theoretical ICCD is chosen between 0.5 and 1.5 μs (shaded areas in Figure 3a and b) that embraces an optimal SNR for all

(13) Voigtman, E. *Appl. Spectrosc.* **1991**, *45*, 237−241.

(14) Neuhauser, R. E.; Panne, U.; Niessner, R.; Petrucci, G. A.; Cavalli, P.; Omenetto, N. *Anal. Chim. Acta* **1997**, *346*, 37−48.

(15) Fink, H.; Panne, U.; Niessner, R. *Anal. Chem.* **2002**, *74*, 4334−4342.

Table 1. Limits of Detection (%)[a]

element	line (nm)	experiment LOD (%) short gated ICCD[b]	experiment LOD (%) long gated ICCD[c]	experiment LOD (%) CCD	model LOD (%) short gated ICCD	model LOD (%) CCD
Si	288.16	0.025	0.018	0.022	0.001	0.0007
V	437.92	0.027	0.023	0.022		
Mo	317.03	0.043	0.028	0.029		
Cu	327.39	0.011	0.008	0.009		
Ni	341.47	0.039	0.034	0.025		
Cr	425.43	0.015	0.011	0.008		

[a] Limits of detection (3σ criterion) in low alloy steel matrix (experimental) and aluminium alloy (theoretical). [b] Short gate, 2 μs. [c] Long gate, 50 μs.

concentrations. The results of optimization of a theoretical nongated CCD detector are presented in Figure 3c and d. In computations, the start time of spectral integration is shifted in 50-ns increments from 0 to 2.95 μs (the latter number being the whole simulated plasma life time), while the integration is performed for the remaining time interval. The integrated signal plotted as a function of shift time (Figure 3c) does not exhibit the maximum as in the case of the ICCD detector (Figure 3a); however, the SNR does exhibit the maximum. Based on this, the integration time window for the theoretical CCD is chosen between 0.5 and 3 μs (shaded areas in Figure 3c and d).

The results of *experimental* delay gate optimization for the Si(I) 288.16 nm line are given in Figure 4a and b for the ICCD/echelle system. The ICCD is operated with a fixed gain of 125, which offers the maximum SNR without saturating the detector at any wavelength. The rough optimization is performed by scanning the 1-μs gate in 1-μs increment within the 0−7-μs interval of the plasma emission time. This follows by further optimization by scanning the same 1-μs gate in smaller 200-ns increments within the narrower time interval of 0−3 μs. Using the minimal allowed gate of 1 μs (this was a limitation of our particular echelle/ICCD system), an optimal delay/gate combination for the used combination of analytical lines is found to be 1.1 μs/2 μs that is illustrated in Figure 4a and b as shaded areas. The delay corresponds to the maximum of the SNR from Si(I) 288.16 nm. Note, that this window includes the maximum of the SNR curve (Figure 4b) but does not include the maximum of the signal curve (Figure 4a) because this latter maximum corresponds to a higher noise level.

Shown in Figure 4c and d are the signal and SNR temporal profiles measured by the chopped CCD system at 288.16 nm. Upon the optimization, the initial cutoff time is shifted step-wisely from 0 to 7 μs in 160-ns increments while the total exposure time of the CCD is set at 1 s corresponding to accumulation of 10 pulses. The optimal cutoff time for the CCD is found to be the same as that for the ICCD, i.e., 1.1 μs.

Theoretical SNR and LOD. Ten theoretical spectra with superimposed noise are averaged for each concentration of Si in the Al matrix. This simulates an analytical signal taken as an average of 10 laser pulses. Because laser−matter interaction is not included in the theoretical model, we cannot take into account fluctuations in laser intensity. In experiments, these fluctuations can, however, be significant (5−10%), imposing additional noise on a signal. On the other hand, this noise is not essential for comparison of the detectors because it is the same for both detectors and it does not affect their transmission function.

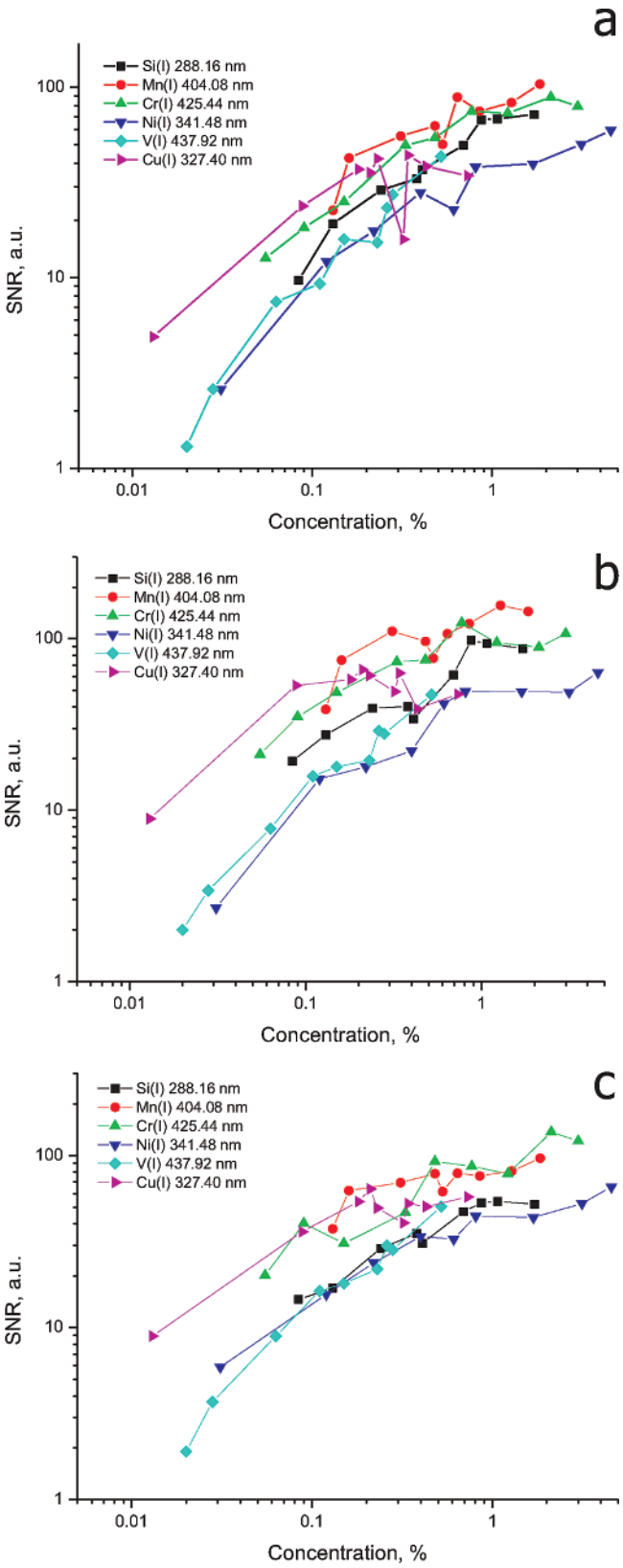

Figure 6. Experimental SNRs obtained with 2-μs gate ICCD (a), 50-μs gate ICCD (b), and CCD with a mechanical chopper (c). The delay time of 1.1 μs is the same for all graphs.

For the theoretical CCD and ICCD, computed calibration curves for the Si(I) emission at 288.16 nm are shown in Figure

5a, where the 3σ level is indicated by dashed horizontal lines. Figure 5a demonstrates that limits of detection for the theoretical ICCD and that for the theoretical CCD are very close, with a slight advantage for the CCD. The absolute values of these LODs cannot, however, be taken as real prediction of experimental sensitivity because the model describes a vacuum plasma, whereas the experiment is carried out in air. As the initial conditions for calculations are chosen quite arbitrarily, the agreement of theoretical LODs with the experimental LODs (see Table 1) is purely accidental. However, the calculated values of LODs still can adequately illustrate the experimental situation as they reflect the response of the two detectors on a transient signal. Figure 5b provides additionally the computed SNRs as a function of concentration. Again, the results are slightly better for the CCD than for the ICCD. This can simply be explained by the fact that the total signal accumulation time with the CCD is larger than that with the ICCD. Not surprisingly, in the limit of photon noise, the SNR, increasing as a square root of the accumulated signal, is higher for longer accumulation times, i.e., for the CCD. Based on our simulations, we conclude that the CCD should provide, as a minimum, similar detection capability as compared to the ICCD.

Experimental SNR and LOD. Each experimental spectrum is taken under atmospheric conditions with an accumulation of 10 laser pulses. The calibration curves for different emission lines are established from measurements at 11 different locations on the sample in order to avoid problems associated with sample heterogeneity. The average of 11 measurements is taken as an analytical signal.

In addition to a short, 2-μs gate of the ICCD, we also used a long, 50-μs gate starting at the same delay time. The gate width of 50 μs is close to the plasma decay time under atmospheric conditions; hence, analogous to the CCD, the 50-μs gate ICCD will effectively integrate the entire plasma emission after the specified initial delay. A precision of the chopper cutoff time is limited by the mechanical jitter which is on the order of 100 ns. Calibration plots are shown in Figure 5c for Si 288.16-nm emission line, same as in the theoretical model. Figure 5c reveals immediately that limits of detection are similar for both the CCD and ICCD, being slightly better for the long-gated ICCD. This result is confirmed by our theoretical prediction and contradicts the earlier results[3,4] where at least 1 order of magnitude worse detection limits were reported for the CCD compared to those of the ICCD. As observed in Figure 5d, the SNRs of the CCD and ICCD with both short and long gates differ insignificantly, especially for low concentrations. The saturation of both the calibration curves (Figure 5c) and SNRs (Figure 5d) observed at high concentrations can be explained by the strong self-absorption of the Si(I) 288.16-nm line. For both detectors, the theoretical and experimental calibration curves show identical saturation behavior. Figure 6a−c summarizes all SNRs obtained with the ICCD (short and long gates) and the CCD. Notably but not surprisingly (see Experimental Section), the SNRs are similar for the two detectors over the entire concentration range. Limits of detection of elements under the study are summarized in Table 1. A close inspection of Table 1 does not reveal any substantial difference in the performance of the ICCD, either with long or short gates, and the CCD. Moreover, in some cases (Cr, Ni, V), LODs achieved with the CCD are even better than those obtained with the ICCD. This result is in good agreement with our simulations as well as the estimates given in refs 7 and 8. Note that the limits of detection shown in Table 1 are somewhat higher than those reported in the literature; achieving record-low detection limits was not the goal.

CONCLUSIONS

We demonstrated, both theoretically and experimentally, that there is no substantial difference in performance of intensified (ICCD) and nonintensified (CCD) detectors employed for spectrochemical analysis of laser-induced plasmas. The CCD detector was used in combination with a mechanical chopper, which provided a controllable data acquisition delay with respect to the laser pulse. Signal-to-noise ratios and limits of detection obtained with the CCD for Si, Ni, Cr, Mo, Cu, and V in the steel samples were comparable or even better than those obtained with the ICCD. This result was also confirmed by computer simulations of detector responses to a transient signal. A nonintensified CCD with some sort of a controllable trigger of data acquisition is therefore an appropriate choice for LIBS as it provides the same sensitivity of analysis as an intensified CCD detector. At a lower cost, the chopped CCD system has in addition a better dynamic range, which is of utmost importance for utilizing echelle systems in real applications.

ACKNOWLEDGMENT

We thank the LTB team for their support. We thank the Deutsche Forschungsgemeinschaft for financial support. The support by the U.S. DOE-DE-F602-99ER 14960 grant is greatly appreciated.

SUPPORTING INFORMATION AVAILABLE

Additional information as noted in text. This material is available free of charge via the Internet at http://pubs.acs.org.

Received for review November 14, 2006. Accepted April 12, 2007.

AC0621470